Open NASA Blade Models for Nonlinear Dynamics Simulations

Solène Kojtych, Alain Batailly

POLYTECHNIQUE MONTRÉAL
UNIVERSITÉ D'INGÉNIERIE

LABORATOIRE D'ANALYSE VIBRATOIRE ET ACOUSTIQUE

Open NASA Blade Models for Nonlinear Dynamics Simulations

Solène Kojtych[1], Alain Batailly[1]

Abstract
This contribution presents a catalogue of open turbomachinery blade models dedicated to nonlinear dynamics simulations. Based on a specifically developed in-house computer code, 3D CAD models and finite element models of multiple-circular-arc NASA airfoils are generated. Both the in-house code and the models are made freely accessible online. To cover a wide range of geometries, 39 blades are considered from different stages and with different aspect ratios. It is expected that this blade catalogue will provide an opportunity for the direct comparison of recently developed methodologies relative to nonlinear vibration phenomena in turbomachines, including rubbing events and blade-tip/casing contacts. To this end, the paper also contains original results for some of the most emblematic NASA blades, with an emphasis on nonlinear interaction maps and a detailed presentation of redesign operations to mitigate high amplitude of vibrations when blade-tip/casing contacts occur.

Keywords
open blade model, NASA blades, blade catalogue, nonlinear structural interactions, blade-tip/casing contacts

1 - Department of Mechanical Engineering, École Polytechnique de Montréal, P.O. Box 6079, Succ. Centre-Ville, Montréal, Québec, Canada H3C 3A7

Modèles ouverts d'aubes NASA pour simulations dynamiques non linéaires

Solène Kojtych[1], Alain Batailly[1]

Résumé
Cet article présente un catalogue de modèles ouverts d'aubes de turbomachines dédiés à des simulations dynamiques non linéaires. À partir d'un code laboratoire spécifiquement développé pour cet usage, des modèles CAO 3D et des maillages éléments finis d'aubes NASA, définies par des profils de type arcs circulaires multiples, sont générés. Le code et les modèles générés sont rendus disponibles en ligne en libre accès. Pour couvrir une large gamme de géométries, 39 aubes d'allongements variés, issues de différents étages, sont considérées. Ce catalogue d'aubes devrait permettre de comparer directement des méthodologies récentes relatives aux phénomènes vibratoires non linéaires dans les turbomachines, tels que les frottements et les contacts aube/carter. À cette fin, ce travail contient également des résultats originaux pour certaines des aubes NASA les plus emblématiques, en mettant l'accent sur les cartes d'interactions non linéaires et sur une présentation détaillée d'un processus de reconception visant à atténuer les vibrations de grande amplitude lorsque des contacts aube/carter se produisent.

Mots-clés
modèle d'aube ouvert, aubes NASA, catalogue d'aubes, interactions structurelles non linéaires, contacts aube/carter

1 - Département de génie mécanique, École Polytechnique de Montréal, P.O. Box 6079, Succ. Centre-Ville, Montréal, Québec, Canada H3C 3A7

1 Introduction

Bladed components are key elements of aircraft engines and gas turbines. From an industrial standpoint, their design is essentially an optimization problem driven by aerodynamics considerations [1] while structural aspects are often limited to a set of constraints [2, 3]. However, over the past decade, the increased pressure on manufacturers to increase efficiency and lower emissions [4] is slowly changing the game. Indeed, major avenues considered for efficiency improvements include lighter materials and a minimization of aerodynamic leakage flows [5]. When applied to bladed components, the former yields a geometrically nonlinear behavior [6] while the latter favors nonlinear structural interactions, such as blade-tip/casing contacts [7]. In the end, nonlinear structural interactions that were often only considered in accidental configurations must now be accounted for in nominal conditions. This has very significant ramifications on blade design procedures, notably due to the fact that there is no unified theoretical framework for the nonlinear analysis of structural components [8, 9]. That is the reason why, over the past years, engineers and researchers have developed several tools and methodologies dedicated to the numerical simulation, the analysis and eventually the prediction [10, 11, 12, 13] of nonlinear structural interactions.

In addition to the theoretical [8] and numerical [14] challenges inherent to the development of robust and efficient methodologies, researchers are facing a major roadblock related to the confidentiality of industrial blade models' mechanical properties. Indeed, when they are published, results are normalized and mechanical models are not shared. This makes it almost impossible to reproduce results and to compare different methodologies. This is a challenge that researchers in the field of computational fluid dynamics (CFD) faced about thirty years ago. At that time, several competitive developments of CFD software packages called for the use of identical blade profiles in order to compare numerical predictions. NASA rotor 37 [15], an open blade geometry for which a vast amount of experimental data was also available [16], became—alongside other blade geometries designed by NASA—a typical case study for CFD analysis.

Recently, a variety of numerical investigations in structural dynamics underlined the very rich and intricate dynamics response of several NASA blades, including rotor 37 [13, 17] and rotor 67 [18], when they undergo structural contacts at their tip. Based on these observations, a Python code [19] was published to allow anyone to build NASA rotor 37's computer-aided design (CAD) model from the multiple-circular-arc (MCA) profile parameters provided in the original NASA report [15]. Within a couple of years, several researchers used this open mechanical model to illustrate or test their methodologies [20, 21, 22, 23], thus highlighting the critical need for open structural blade models.

Acknowledging the critical need for providing researchers with a large variety of open structural blade models, this article puts forward three major elements. (1) An open source Python code is provided. This Python 3 code builds on the Python 2 code [19] dedicated to NASA rotor 37: several issues have been corrected and it has been expanded to a much more versatile tool making it possible to build the CAD models of 40+ NASA blades based on their MCA profile parameters. (2) A catalogue of 39 open NASA blade models is also provided. For each blade, a CAD model, a finite element (FE) mesh and a reduced order model are provided. (3) Finally, this paper presents a sample of typical results obtained for certain NASA blades with respect to nonlinear dynamics time integration-based simulations and blade design optimizations.

The second section of the paper is dedicated to the presentation of the blade model generation code, referred to as `OpenMCAD` (open blade model generator from MCA parameterization to CAD model). In the third section, the focus is put on the presentation of the catalogue of open blade models dedicated to nonlinear structural analyses. Then, in the fourth section, a sample of original results obtained on three blade models with respect to their nonlinear dynamics response are presented with the intent to underline the applicability of the proposed blade models to the analysis of nonlinear structural interactions.

2 `OpenMCAD`: Blade model generation code

The blade model generation code [24] allows to automatically build a blade CAD model and FE mesh from the MCA profile parameters provided in original NASA reports.

(a) For rotor 35

RP	PERCENT SPAN	RADII RI	RO	BLADE ANGLES KIC	KTC	KOC	DELTA INC	CONE ANGLE
TIP	0.	25.248	24.511	62.55	62.99	53.21	2.09	-15.764
1	5.	24.916	24.221	61.52	61.84	52.53	2.41	-14.327
2	10.	24.571	23.931	60.55	60.74	51.87	2.72	-12.780
3	15.	24.224	23.642	59.80	59.85	51.23	2.96	-11.326
4	30.	23.163	22.772	58.34	57.74	48.54	3.41	-7.137
5	50.	21.726	21.613	56.16	54.31	44.26	4.21	-1.890
6	70.	20.221	20.454	53.70	49.53	39.16	5.51	3.545
7	85.	19.019	19.584	52.28	47.30	33.31	6.56	8.150
8	90.	18.596	19.294	52.00	46.85	30.96	6.86	9.887
9	95.	18.158	19.005	51.82	46.50	28.36	7.18	11.763
HUB	100.	17.780	18.715	51.69	46.24	25.70	7.46	12.787

RP	BLADE THICKNESSES TI	TM	TO	AXIAL DIMENSIONS ZI	ZMC	ZTC	ZO
TIP	.025	.175	.025	.698	2.410	2.379	3.308
1	.027	.187	.027	.635	2.361	2.345	3.354
2	.028	.199	.028	.576	2.313	2.301	3.398
3	.029	.212	.029	.529	2.269	2.242	3.438
4	.032	.252	.032	.417	2.188	2.051	3.542
5	.037	.305	.038	.280	2.133	1.896	3.701
6	.042	.361	.043	.129	2.045	1.749	3.884
7	.047	.408	.047	.058	1.992	1.715	4.007
8	.048	.425	.049	.037	1.967	1.646	4.046
9	.050	.443	.050	.017	1.940	1.579	4.082
HUB	.051	.458	.051	.000	1.915	1.520	4.118

Figure 1. MCA profile parameters for rotor 35, from [26].

2.1 Key characteristics

The code `OpenMCAD` is open source and freely available online [24] under the GNU public license. It is provided with examples of input parameters and output models.

`OpenMCAD` builds on a previously released Python 2 code [19] dedicated to the modeling of NASA rotor 37, based on the original Fortran IV NASA code related to MCA blade generation [25]. Although the previous Python 2 code and `OpenMCAD` share a similar structure, significant developments and modifications have been made in `OpenMCAD` to go beyond the limitations of the initial Python 2 code to make it a versatile blade modeling tool, applicable to most of the available NASA fan and compressor blade models.

Main modifications and improvements of `OpenMCAD` are: (1) a more robust and versatile CAD generation procedure that has been validated on 40+ blade models, (2) the correction of an error that caused the inversion of suction and pressure sides at intermediate computation steps, (3) the computation of CAD models and FE meshes in SI units to promote their compatibility with simulation routines, and (4) the transcription of the code from Python 2 to Python 3 to ensure its sustainability and portability. A complete list of modifications may be found in the code documentation.

2.2 Input blade parameters

Input blade parameters read by the code must rely on the blade parameterization described by Crouse *et al.* [25] and used in original NASA reports: a blade is represented by N MCA profiles describing its intersections with N conical surfaces distributed along its height.

A MCA profile is defined in an unwrapped conical surface by three curves: the chordline, the pressure side and the suction side. Each curve is composed of two circular arcs meeting at a transition point. Profile parameters are defined at four reference points (leading edge, trailing edge, transition point and maximum thickness point) and include radial and axial coordinates, blade thickness and blade angle, defining the orientation of the centerline at the considered point. In total, 11 parameters are required to define one profile. For all blades considered in this work, the MCA profile parameters may be found in corresponding NASA reports. For instance, the MCA profile parameters of rotor 35 are given in Fig. 1.

The positioning of profiles on the conical surfaces is controlled by a stacking line. In the code, the stacking line may be: (1) a straight line defined by global lean and sweep angles, as in the original formulation proposed by Crouse *et al.* [25], or (2) a spline curve, controlled by specific sweep and lean angles for each profile. This latter option

allows more flexibility in the stacking of profiles, which may be of great interest for design purposes. Nonetheless, for all blades generated in this article, in order to ensure consistency with original NASA reports, profiles are stacked along the radial direction.

2.3 Main steps

The execution of the code may be decomposed into four main steps: (1) smoothing of the input parameters, (2) computation of 3D point clouds, (3) generation of the CAD model, and (4) generation of the FE mesh.

smoothing of input parameters: some profile parameters may be smoothed along the blade height to improve the smoothness of the subsequent CAD model. More specifically, for each of these parameters, the N parameter values—one per profile— are used to compute a cubic polynomial fitting with respect to the radial position. Smoothed values are given by this fitting and a new parameters file is thus generated for each profile.

point clouds computation: from the smoothed MCA profile parameters, 3D Cartesian coordinates of points describing each profile are computed. This results in N point clouds, that are split in two files describing, respectively, the pressure side and the suction side of the profile.

CAD model generation: the N point clouds are read by the open-source software package Salome 9.6[1]. For each profile, points of the suction and pressure sides are each interpolated. Based on the obtained profile curves, two spline surfaces are computed to model the pressure and suction faces of the blade. Considering an adaptative tolerance, coincident edges are detected and the two faces are sewed into a single side surface. The hub and top faces are generated by filling the holes to obtain a shell, which is then transformed into a solid. As an example, the CAD model computed for rotor 35 is shown in Fig. 2.

FE mesh generation: all blade edges are discretized in n_{seg} segments. The two side faces are consistently meshed with quadrangles and the top and hub faces are meshed with triangles, whose area is limited by a value relative to the blade chord. Thus, the blade is meshed with quadratic pentahedrons. The FE mesh related to rotor 35 is shown in Fig. 2; a value of $n_{\text{seg}} = 38$ segments was found sufficient to ensure the convergence of the mesh and leads to a mesh with 10 236 pentahedrons. The same n_{seg} value was considered for all blades of the catalogue.

The computation time[2] of the four steps is about 15 s per blade.

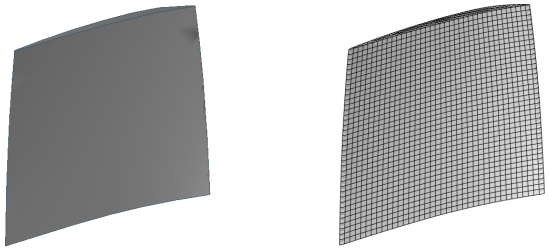

(a) CAD model **(b)** FE mesh

Figure 2. Reference blade rotor 35.

3 Blade catalogue

Making use of the blade model generation code `OpenMCAD`, a catalogue of 39 open NASA blade models is made available online [27]. Most of the blade geometries were initially defined in the context of research programs conducted at NASA Lewis Research Center in the 70's and 80's. While these blades have been extensively used for a variety of CFD simulations, their use for structural analyses remains very limited. Yet, preliminary results obtained in the context of nonlinear vibration analyses also underlined their very rich and intricate dynamics as they undergo

[1] `https://www.salome-platform.org/`

[2] On a PC with 8 Intel Core i7-7700T CPU (4.20GHz) processors.

Table 1. Material properties.

material	18-Ni-200-maraging	Ti-6Al-4V
Young's modulus [Pa]	1.8×10^{11}	1.08×10^{11}
density [kg·m^{-3}]	8000	4400
Poisson's ratio	0.3	0.34

structural contacts along their tip [13, 17, 18]. For that reason, these blades could serve as ideal benchmarks for recently developed and future numerical strategies focusing on nonlinear structural interactions.

The provided blades are listed in Table 2. They relate to both compressor and fan stages and exhibit a wide range of geometries and height, from around 5 cm to 15 cm. The catalogue notably includes the emblematic models rotor 37 [15] and rotor 67 [28].

Blade CAD models and FE meshes obtained directly from the blade generation code `OpenMCAD` are referred to as *ref-blades* (for reference blade models). In addition, the catalogue also features CAD models and FE meshes for the same NASA blades that are related to a distinct in-house parameterization [29, chap. 4]. In order to avoid any confusion, the latter blades are labeled *ip-blades* (for initial parameterized blades), where *initial* refers to the starting point of design optimization procedures [18] that may be carried out[3]. Finally, for each ip-blade, a reduced order model (ROM) obtained with the Craig-Bampton component mode synthesis technique is provided. These ROMs are used in the following for a variety of numerical simulations. Details on each blade model are given on a dedicated wiki website[4].

3.1 Reference blades

Based on the MCA profile parameters of each blade of the catalogue, `OpenMCAD` is used to generate the associated reference CAD models and FE meshes. CAD models are provided as `step` files and meshes are given both in human readable `unv` format and binary `med` format. The latter may be used in Salome or in the open-source FE code Code Aster[5].

Beside of these models, key pieces of information for each blade are provided on the Laboratory for Acoustics and Vibration Analysis's wiki website[6]. In particular, one may find the input parameter files used in `OpenMCAD` for model generation as well as a link toward original NASA reports. When available, blades' aerodynamic and material extracted from original or subsequent reports are also provided: a maraging steel 18-Ni-200 and a titanium alloy Ti-6Al-4V are mentioned in some NASA reports, identified in the third column of Table 2. When blade material is not provided in reports, the same maraging steel is chosen for compressor blades and the titanium alloy is considered for fan blades, as mentioned in Table 2. Detailed material properties are taken from previous studies [17, 30] and summarized in Table 1. Finally, the first three eigenfrequencies of the ref-blades are computed from the FE meshes and provided for the sake of completeness.

3.2 Initial parameterized blades

With the increased interest in nonlinear structural interactions within aircraft engines and the development of more efficient numerical strategies dedicated to their prediction, there is a push toward accounting for these interactions early in blade design stages to prevent costly redesign operations [31]. Recently, a few publications addressed this topic [18, 22, 23] and parameterizations well suited for mechanical analyses have been proposed [23, 29]. In particular, a redesign methodology has been developed and applied to compressor blades with the intent to increase their robustness to blade-tip/casing contacts [18], featuring promising results on NASA rotor 37.

The proposed blade catalogue could play an important role in assessing the versatility and the relevance of such redesign operation. Indeed, the redesign of diverse blade models is required to get a better understanding of key

[3] In-depth comparisons between ref-blade models and ip-blade models have been carried out in a previous work, the almost perfectly identical vibration behavior was notably underlined [29, chap. 4].

[4] `https://lava-wiki.meca.polymtl.ca/public/accueil`

[5] `https://www.code-aster.org/`

quantities of interest for different nonlinear structural interactions. It will also play a key role in the definition of relevant performance criteria. This is the reason why ip-blades—that are consistent with the parameterization used for redesign operations [18]—are provided in addition to the ref-blade models.

3.2.1 CAD model and FE mesh

From each ref-blade model, a reverse engineering method [29] is applied to acquire blade parameters consistent with the in-house parameterization. The numerical tool previously introduced in the literature [29] is then used to build the associated initial parameterized CAD model and FE mesh.

In a previous publication [29], particular attention has been paid to demonstrating the high fidelity of ip-blade models with respect to the ref-blade models, with an emphasis on: (1) modal properties and (2) dynamic response in both linear and nonlinear configurations. For comparison purposes, the first three eigenfrequencies of ip-blades are also indicated on the wiki website. A relative error with the eigenfrequencies of the ref-blade of less than 1.7% is observed for all blades.

3.2.2 Reduced order model

The computational cost associated to nonlinear dynamics simulations typically prevents the use of full FE models. Component mode synthesis (CMS) techniques such as the Craig-Bampton technique [32] are thus classically used in nonlinear dynamics. While a vast number of more recent model reduction techniques have been proposed [33, 34, 35], the Craig-Bampton method remains very popular due to the fact that: (1) it allows, by design, to retain physical degrees of freedom within the reduced space, which is advantageous for contact management, and (2) it is less sensitive to conditioning issues that may arise with other CMS techniques.

To ease further structural dynamics analysis of catalogue blades, a Craig-Bampton ROM [32] of each ip-blade is computed from the FE mesh. The model is provided as a `mat` file, readable with both Python and Matlab, and contains the reduced mass and stiffness matrices.

To compute the ROM, the material properties identified for the ref-blade are considered and the blade hub is assumed to be clamped. Eight boundary nodes evenly distributed along the intersection of the tip face and the pressure side are considered. These nodes are identified in a distinct group in the mesh files. Three degrees of freedom at each boundary node and 10 modal degrees of freedom are considered, leading to a reduced order model featuring 34 degrees of freedom. Centrifugal effects are neglected, *i.e.* the stiffness matrix is independent from the blade angular speed. Convergence of the ROM was checked by comparing its eigenfrequencies to those of the full FE model. A relative error of less than 1% was observed on the first three eigenfrequencies reported on the wiki website.

Table 2. Open blade catalogue.

rotor blade model	NASA report	material
1	[36]	18-Ni-200-maraging
3	[37]	18-Ni-200-maraging [37]
4	[38]	18-Ni-200-maraging [38]
5	[39]	18-Ni-200-maraging [39]
6	[40]	18-Ni-200-maraging
7	[41]	18-Ni-200-maraging
8	[42]	Ti-6Al-4V
11	[43]	Ti-6Al-4V
12	[44]	18-Ni-200-maraging
14	[45]	18-Ni-200-maraging
15	[46]	Ti-6Al-4V [46]
16	[47]	Ti-6Al-4V
17	[48]	Ti-6Al-4V
18	[49]	Ti-6Al-4V
20	[50]	Ti-6Al-4V
21	[51]	Ti-6Al-4V
23B	[52]	Ti-6Al-4V
24A	[52]	18-Ni-200-maraging
25A	[52]	18-Ni-200-maraging
26B	[52]	18-Ni-200-maraging
27A	[52]	18-Ni-200-maraging
28B	[52]	18-Ni-200-maraging
35	[53]	18-Ni-200-maraging [26]
36	[54]	18-Ni-200-maraging [26]
37	[15]	18-Ni-200-maraging [26]
38	[55]	18-Ni-200-maraging [26]
51A	[56]	Ti-6Al-4V
51B	[57]	Ti-6Al-4V
52	[58]	Ti-6Al-4V
53	[59]	Ti-6Al-4V
54	[60]	Ti-6Al-4V
55	[61]	Ti-6Al-4V
65	[62]	Ti-6Al-4V [62]
66	[63]	Ti-6Al-4V
67	[28]	Ti-6Al-4V
68	[28]	Ti-6Al-4V
74A1	[64]	Ti-6Al-4V [64]
74A2	[64]	Ti-6Al-4V [64]
74A3	[64]	Ti-6Al-4V [64]

4 Nonlinear dynamics analyses

This section provides a series of original results obtained from the analysis of some of the NASA blades provided in the catalogue. Typical analyses related to blade-tip/casing contacts—specifically rubbing interactions—are here considered based on linear FE models consistent with the small perturbation framework. First, it is shown that the provided mechanical models are well suited for nonlinear dynamics analyses. Then, it is underlined that the

dynamics of the selected blades is very complex and is, to the best of the author's knowledge, representative of the most sophisticated reported vibration behaviors in the literature. While only a sample of available results are provided in the paper for the sake of conciseness, the authors intend to regularly publish additional benchmark results on the Laboratory for acoustics and vibration analysis's wiki website[6] so as to provide a full list of numerical benchmark results for each blade of the catalogue.

The compressor blade rotor 35 [53], the fan blade rotor 68 [28] and the compressor blade rotor 74A2 [64] are selected as they feature very distinct geometries. The CAD models of ip-blades are depicted in Fig. 3. Approximated blade heights are given in Tab. 3 along with aspect ratios and nominal speeds taken from NASA reports. The first three free vibration modes are also identified by modal analysis; 1B denotes the first bending mode, 1T the first torsion mode and 2B the second bending mode.

Table 3. Characteristics of selected ip-blades.

rotor	35	68	74A2
blade height [cm]	7.5	10.9	8.4
aspect ratio	1.19	1.89	1.17
nom. speed[rad·s^{-1}]	1800	1680	1680
modes order	1B, 1T, 2B	1B, 2B, 1T	1B, 1T, 2B

4.1 Dynamic analysis of initial parameterized blades

4.1.1 Simulation strategy

The amplitudes of vibration of each blade as it undergoes contact interactions are predicted with time integration simulations using the reduced order model provided in the catalogue, see Section 3.2. Main simulation parameters are summarized in Tab. 4, remaining parameters are consistent with those used in a previous publication [29].

For each blade, simulations are run for a large range of angular speeds right below their nominal speed, where several interactions between free vibration modes and engine orders (usually 4 to 8) are linearly predicted. In particular, the intersection between the first bending mode and the fourth engine order, which often yields high vibration magnitudes when blade-tip/casing contacts are considered, belongs to the angular speed range. Simulations are run at each integer value of ω in the range. In order to reach the steady state, 200 tours are simulated at each speed ω and a time step of 10^{-7} s is considered. Contact between the tip of the blade and the surrounding casing, assumed to be perfectly rigid, is initiated through an ovalization of the casing, thus yielding two privileged symmetric contact areas, referred to as lobes. As the blade-tip clearance at rest is mentioned in NASA reports only for rotor 68, clearances for rotor 35 and rotor 74A2 are defined empirically. The height of the lobes is relative to the clearance.

Table 4. Main simulation parameters for rotor 35, rotor 68 and rotor 74A2.

rotor	35	68	74A2
speed range [rad·s^{-1}]	[850; 1700]	[410; 1235]	[820; 1645]
tip clearance [m]	5×10^{-4}	6×10^{-4}	3×10^{-4}
lobe height [m]	6.25×10^{-4}	4.2×10^{-4}	3.75×10^{-4}

4.1.2 Results

For each speed ω, boundary nodes displacements over the 200 blade revolutions are computed with an in-house simulation tool, based on a published numerical strategy [10]. It has been checked that steady states have been reached for each simulation. For a given node, an interaction map may be drawn to represent the steady-state frequency content of the displacement signal with respect to the speed ω. In this work, for each speed ω, a Fast

[6] https://lava-wiki.meca.polymtl.ca/public/accueil

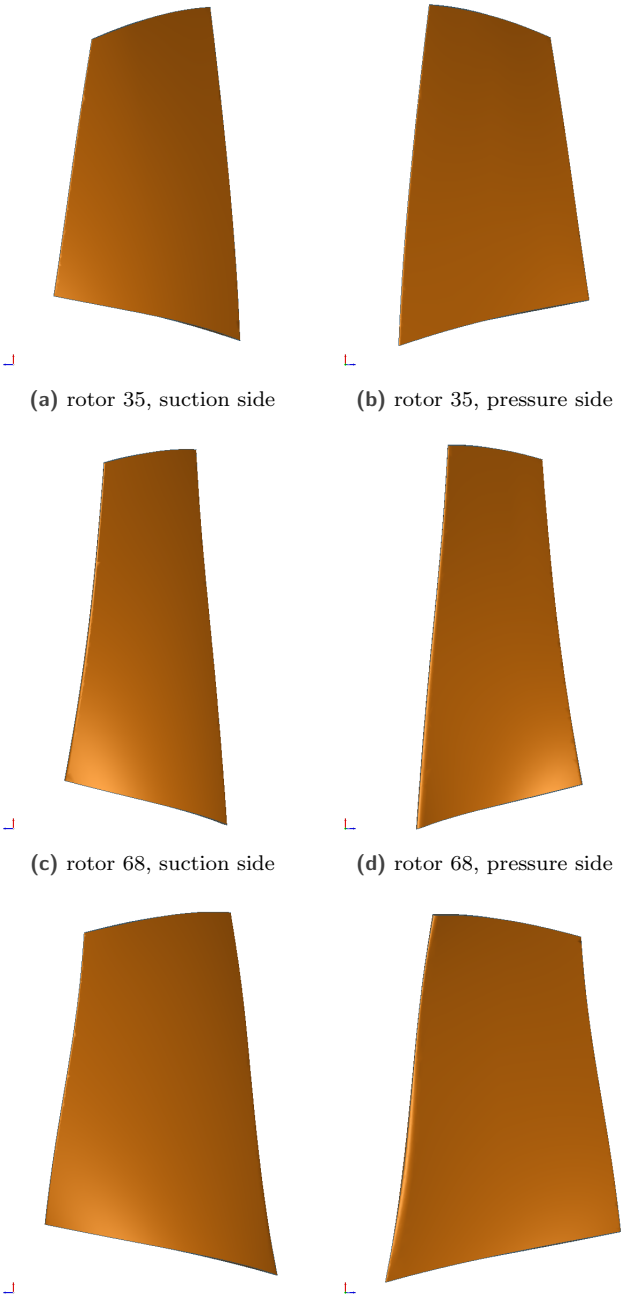

(a) rotor 35, suction side **(b)** rotor 35, pressure side

(c) rotor 68, suction side **(d)** rotor 68, pressure side

(e) rotor 74A2, suction side **(f)** rotor 74A2, pressure side

Figure 3. CAD models of selected ip-blades.

Fourier Transform of the leading edge radial displacement over the last 40 blade revolutions is computed. The juxtaposition of the spectra computed for each ω yields the interaction maps depicted in Fig. 4. The magnitude of the spectra is represented with a logarithmic color map: neglectable magnitudes (¡10^{-5} m) are in black and maximal amplitudes are in white. The frequencies of the first three vibration modes are depicted with white lines (═) and

relevant engine orders are shown with dashed lines (- - -).

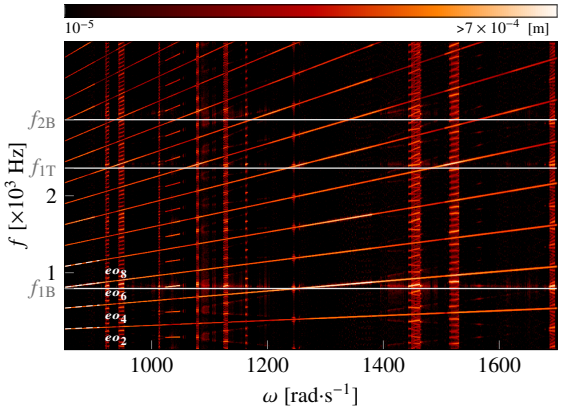

(a) rotor 35

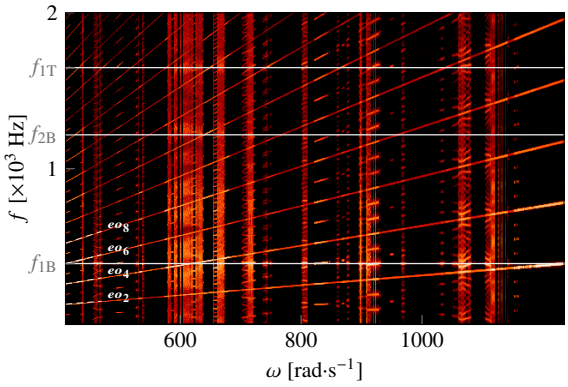

(b) rotor 68

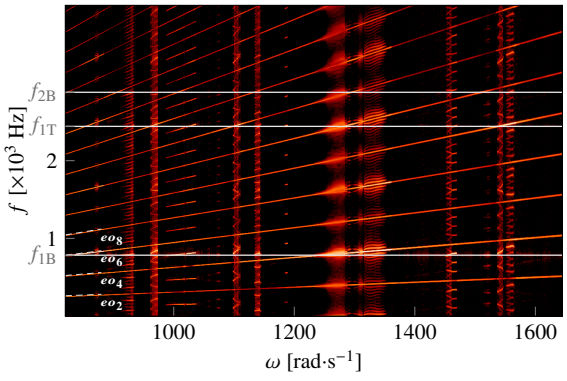

(c) rotor 74A2

Figure 4. Interaction maps for selected ip-blades.

Overall, the interaction maps obtained for rotor 35, 68 and 74A2 ip-blades underline the intricacy of their dynamics as blade-tip/casing contacts occur. In particular, as previously observed in the literature [17], the lack of abradable coating promotes vibration behaviors involving higher frequency modes with potentially low amplitudes of vibrations. This is the reason why so many complex vibration patterns are evidenced throughout the interaction maps.

See, for instance, $\omega \in [1000; 1150]$ rad·s^{-1} for rotor 35, $\omega \in [800; 950]$ rad·s^{-1} for rotor 68 and $\omega \in [900; 1150]$ rad·s^{-1} for rotor 74A2. Interestingly, for angular speeds slightly above that of the intersection between mode 1B and engine order 4, very distinct vibration behaviors are evidenced for each blade. For rotor 35, a progressive increase in vibration amplitudes along engine order 4 is predicted with no significant contribution of other modes. However, for rotor 68, the time integrator seems to provide very different solutions from an angular speed to the next, thus hinting at the possible coexistence of many different types of solution branches. Finally, for rotor 74A2, it seems that the intersection between mode 1B and engine order 4 also corresponds to the intersection between mode 1T and engine order 12, which leads to complex vibration patterns dominated by these two modes.

4.2 Blade shape optimization

A recently developed redesign methodology allows to update the blade shape with respect to a performance criterion associated to structural dynamics. This blade shape update relies on an iterative optimization process. An example of such optimization problem is here considered, where the chosen performance criterion is the clearance consumption, presented in Section 4.2.1. The optimization problem is formulated in Section 4.2.2 and optimization results are given in Section 4.2.3.

4.2.1 Performance criterion

The clearance consumption has been identified as a relevant indicator of the robustness of certain types of blades to contact interactions [17, 18, 22, 23, 65]. The clearance consumption is defined for a node v and a free vibration mode p and denoted $c_{v,p}$; it quantifies the evolution of the tip clearance at this node when the blade vibrates along mode p. In accordance to previous work [18, 23], the performance criterion considered is the clearance consumption at the leading edge of the blade tip along the first bending mode, denoted $c_{LE,1B}$. Clearance consumption computations are conducted with the open source mechanical software package Code Aster[5] and detailed computation steps may be found in previous publications [23, 29, 65].

4.2.2 Problem formulation

For each of the selected NASA ip-blades, the considered optimization problem aims at minimizing the clearance consumption at the leading edge on the first vibration mode. The main characteristics of this problem are presented below and a complete description may be found in a previous publication [18]. Four optimization variables are considered related to the axial sweep and the tangential lean at mid-span and at top of the blade, in agreement with recent published work [17, 18]. This choice advantageously makes it possible to alter the global shape of the blade while considering a limited number of optimization variables.

Bound constraints are considered: axial sweep is constrained between -2 mm and $+2$ mm and tangential lean may vary between $-1.5°$ and $+1.5°$. As these bounds are tight, only small geometrical variations are authorized and the first free vibration mode is thus assumed to remain the first bending mode for all blades at each iteration of the optimization process.

Because the gradient of the clearance consumption is not analytically known, the optimization problem is treated as a blackbox optimization problem. It is solved with the open-source software package NOMAD (v. 3.9.1) [66] which relies on the derivative-free optimization algorithm Mads [67]. This algorithm iteratively proposes sets of blade parameters from which a CAD model and a FE mesh are generated to finally compute the clearance consumption. Four hundred computations of the clearance consumption are allowed for each blade optimization.

4.2.3 Results

The CAD models are computed from optimized parameters returned at the end of the optimization and presented in Fig. 5a, 6a and 7a, superimposed with the CAD models of the ip-blades. The clearance consumptions at all boundary nodes for the three first free vibration modes for both ip-blades (——) and optimized blades (——) are shown in Fig. 5, 6 and 7. Boundary nodes v are indexed from the leading edge (1) to the trailing edge (8). Clearance consumptions used as performance criteria are circled in black. For all blades, it is found that the optimized blades feature a significantly lower value of $c_{LE,1B}$ which confirms the carried out optimization was successful.

More specifically, the presented results provide interesting insight about each of the considered ip-blades:

rotor 35: the optimization process yields an almost zero clearance consumption at the leading edge, see Fig. 5b. Simultaneously, clearance consumptions computed for all other boundary nodes along the blade tip for the first bending and torsion modes are globally significantly lowered. However, clearance consumptions of the optimized blade for the second bending mode are more than doubled in the vicinity of the leading edge, see Fig. 5d. These first results underline the usual trade-off one might have to deal with for such optimization.

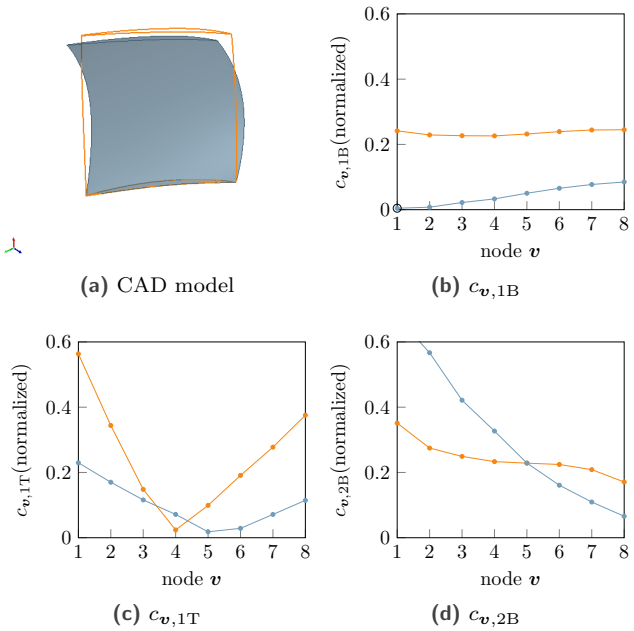

(a) CAD model **(b)** $c_{\boldsymbol{v},1B}$ **(c)** $c_{\boldsymbol{v},1T}$ **(d)** $c_{\boldsymbol{v},2B}$

Figure 5. CAD model and clearance consumptions for initial (——) and optimized (——) rotor 35 blade.

rotor 68: for this fan blade, the optimization process also yields an almost zero clearance consumption at the leading edge, see Fig. 6b. In addition, clearance consumptions for other boundary nodes for modes 1B and 2B are significantly lowered. It is also noticeable that the increases in clearance consumptions for mode 1T, that are mostly located close to the leading edge (nodes 1 to 4), remain very small.

rotor 74A2: results obtained for this blade are noticeable since the clearance consumption of the ip-blade at the leading edge was already very small. Nonetheless, a further lowered clearance consumption is obtained with the optimization process, see Fig. 7b. Clearance consumptions for the first torsion mode are practically unchanged while those of the second bending mode are overall significantly reduced, to the exception of the two boundary nodes closest to the leading edge.

4.3 Dynamic analysis of the optimized blades

Interaction maps obtained for the optimized blades are computed using the same parameters as the ip-blades and depicted in Fig. 8. The contact scenario also remains identical to the one used for the ip-blades so that the only difference between interaction maps plotted in Figs. 4 and 8 are the blade models themselves. A detailed analysis of the consequence of the carried out optimization process on the blades' dynamics response goes beyond the scope of this paper. Nonetheless, there are general trends that seem worth mentioning. With respect to rotor 35, an across-the-board decrease of vibration amplitudes is obtained at the expense of more frequent sophisticated vibration patterns that seem to involve higher frequency modes. For rotor 68, significant decreases of vibration amplitudes related to mode 1B are counterbalanced with significantly increased vibration amplitudes related to mode 2B even though clearance consumptions for that mode were also reduced. Finally, for rotor 74A2, only foe modifications are predicted in the blade dynamics response, which is consistent with the fact that the blade shape was less impacted by the optimization process due to the already very low clearance consumption of the ip-blade.

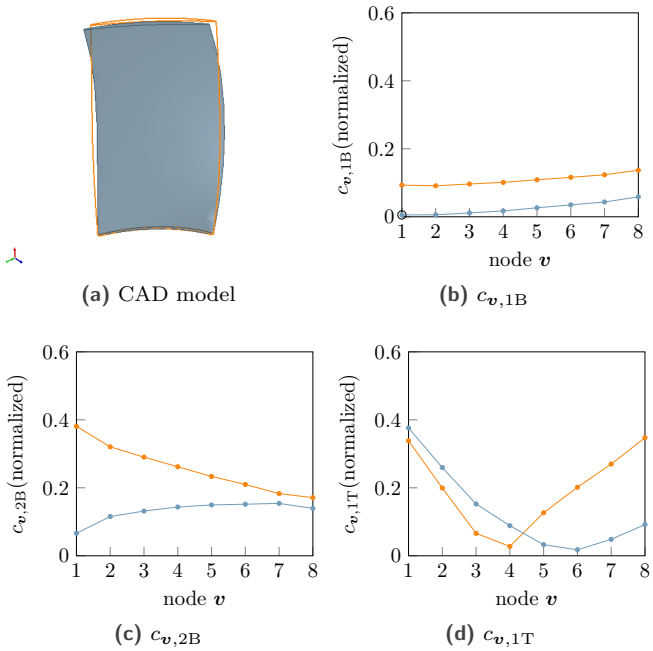

(a) CAD model **(b)** $c_{\boldsymbol{v},1\mathrm{B}}$

(c) $c_{\boldsymbol{v},2\mathrm{B}}$ **(d)** $c_{\boldsymbol{v},1\mathrm{T}}$

Figure 6. CAD model and clearance consumptions for initial (——) and optimized (——) rotor 68 blade.

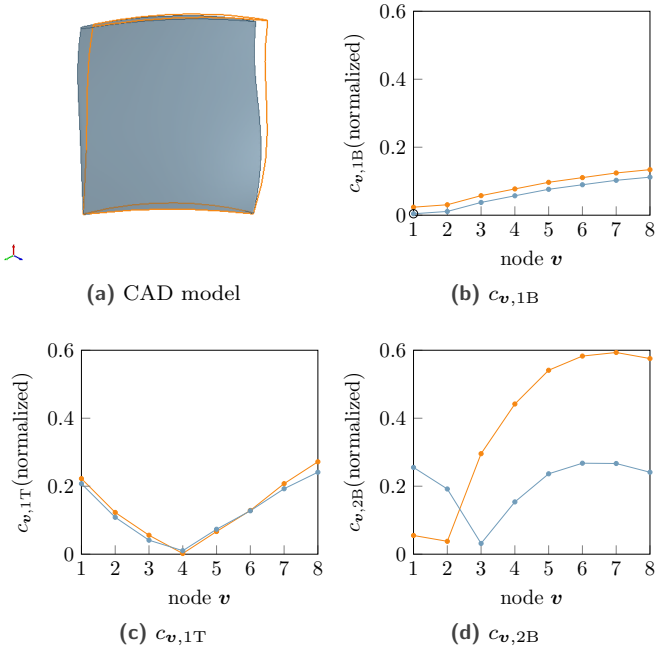

(a) CAD model **(b)** $c_{\boldsymbol{v},1\mathrm{B}}$

(c) $c_{\boldsymbol{v},1\mathrm{T}}$ **(d)** $c_{\boldsymbol{v},2\mathrm{B}}$

Figure 7. CAD model and clearance consumptions for initial (——) and optimized (——) rotor 74A2 blade.

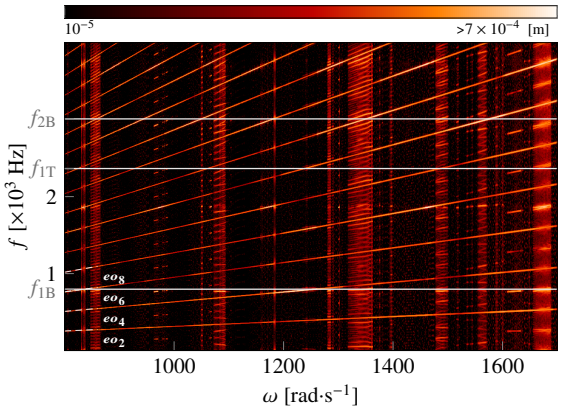

(a) rotor 35

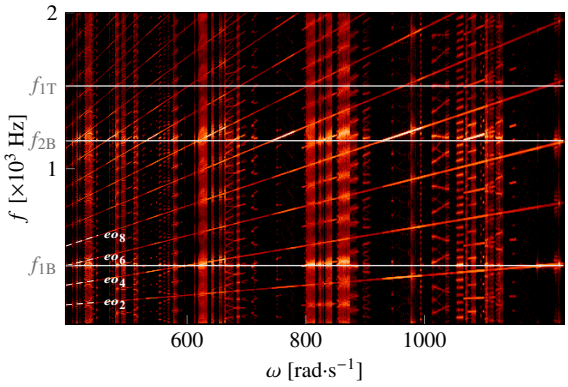

(b) rotor 68

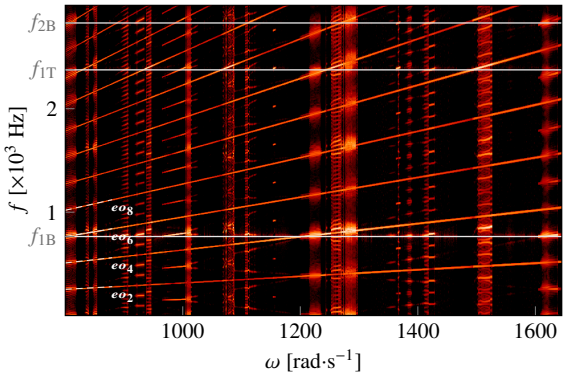

(c) rotor 74A2

Figure 8. Interactions maps for selected optimized blades.

5 Conclusion

This paper presents both the open blade model generation code `OpenMCAD`, and a catalogue of open blade models dedicated to nonlinear dynamics simulations. The free and open diffusion of these two elements intends to promote and to facilitate the comparison of published results obtained with numerical methods dedicated to nonlinear structural interactions. As a starting point, this catalogue is focused on single blade models and samples of

benchmark results related to their dynamics in the context of blade-tip/casing structural contacts are provided. Presented results underline the intricacy of the open blade models' dynamics thus indicating that these models may also be relevant for in-depth structural and design analyses.

Acknowledgments

The authors would like to thank Antoine Lémery for his help with the catalogue preparation and the model generation.

References

[1] Z. Li and X. Zheng. "Review of design optimization methods for turbomachinery aerodynamics". In: Progress in Aerospace Sciences Vol. 93 (2017), 1–23. DOI: 10.1016/j.paerosci.2017.05.003.

[2] M. Aulich and U. Siller. "High-dimensional constrained multiobjective optimization of a fan stage". In: *ASME 2011 Turbo Expo: Turbine Technical Conference and Exposition*. American Society of Mechanical Engineers. 2011, pp. 1185–1196. DOI: 10.1115/GT2011-45618.

[3] C. Chahine, T. Verstraete, and L. He. "Multidisciplinary Design Optimization of an Aero-Engine Fan Blade with Consideration of Bypass and Core Performance". In: *11th World Congress on Structural and Multidisciplinary Optimization*. 2015. URL: http://web.aeromech.usyd.edu.au/WCSMO2015/papers/1087_paper.pdf.

[4] International Energy Agency. *Net Zero by 2050, a roadmap for the global energy sector*. https://www.iea.org/reports/net-zero-by-2050. 2021.

[5] E. Erler, H. D. Vo, and H. Yu. "Desensitization of axial compressor performance and stability to tip clearance size". In: Journal of Turbomachinery Vol. 138, No. 3 (2015). DOI: 10.1115/1.4031865.

[6] E. Delhez, F. Nyssen, J.-C. Golinval, and A. Batailly. "Assessment of Geometric Nonlinearities Influence on NASA Rotor 37 Response to Blade Tip/Casing Rubbing Events". In: Journal of Engineering for Gas Turbines and Power Vol. 143, No. 11 (2021). 111022. DOI: 10.1115/1.4051968. OAI: hal.archives-ouvertes.fr/hal-03286204v1.

[7] H. Ma, F. Yin, Y. Guo, X. Tai, and B. Wen. "A review on dynamic characteristics of blade–casing rubbing". In: Nonlinear Dynamics Vol. 84, No. 2 (2016), 437–472. DOI: 10.1007/s11071-015-2535-x.

[8] A. Thorin, P. Delezoide, and M. Legrand. "Non-smooth modal analysis of piecewise-linear impact oscillators". In: SIAM Journal on Applied Dynamical Systems Vol. 16, No. 3 (2017), 1710–1747. DOI: 10.1137/16M1081506. OAI: hal.archives-ouvertes.fr/hal-01298983.

[9] M. Krack. "Nonlinear modal analysis of nonconservative systems: extension of the periodic motion concept". In: Computers & Structures Vol. 154 (2015), 59–71. DOI: 10.1016/j.compstruc.2015.03.008. URL: https://arxiv.org/abs/2101.00949.

[10] M. Legrand, A. Batailly, B. Magnain, P. Cartraud, and C. Pierre. "Full three-dimensional investigation of structural contact interactions in turbomachines". In: Journal of Sound and Vibration Vol. 331, No. 11 (2012), 2578–2601. DOI: 10.1016/j.jsv.2012.01.017. OAI: hal.archives-ouvertes.fr/hal-00660863.

[11] R. J. Williams. "Simulation of blade casing interaction phenomena in gas turbines resulting from heavy tip rubs using an implicit time marching method". In: *ASME Turbo Expo 2011: Turbine Technical Conference and Exposition*. Vol. 6: Structures and Dynamics, Parts A and B. American Society of Mechanical Engineers. Vancouver, BC, Canada., 2011, pp. 1007–1016. DOI: 10.1115/GT2011-45495.

[12] M. Krack, L. Salles, and F. Thouverez. "Vibration prediction of bladed disks coupled by friction joints". In: Archives of Computational Methods in Engineering Vol. 24, No. 3 (2017), 589–636. DOI: 10.1007/s11831-016-9183-2. OAI: hal.archives-ouvertes.fr/hal-01825517.

[13] Y. Colaïtis and A. Batailly. "Development of a harmonic balance method-based numerical strategy for blade-tip/casing interactions: application to NASA rotor 37". In: Journal of Engineering for Gas Turbines and Power Vol. 143, No. 11 (2021). 111025. DOI: 10.1115/1.4051967. OAI: hal.archives-ouvertes.fr/hal-03286205/.

[14] E. P. Petrov. "Multiharmonic analysis of nonlinear whole engine dynamics with bladed disc-casing rubbing contacts". In: *ASME Turbo Expo 2012: Turbine Technical Conference and Exposition*. Vol. 7: Structures and Dynamics, Parts A and B. Copenhague, Danemark, 2012, pp. 1181–1191. DOI: 10.1115/GT2012-68474.

[15] R. D. Moore and L. Reid. *Performance of Single-Stage Axial-Flow Transonic Compressor With Rotor and Stator Aspect Ratios of 1.19 and 1.26, Respectively, and With Design Pressure Ratio of 2.05*. Tech. rep. NASA-TP-1659. NASA Lewis Research Center Cleveland, OH, United States, 1980. URL: https://ntrs.nasa.gov/citations/19800012840.

[16] J. Denton. "Lessons from rotor 37". In: Journal of Thermal Science Vol. 6, No. 1 (1997), 1–13. DOI: 10.1007/s11630-997-0010-9.

[17] E. Piollet, F. Nyssen, and A. Batailly. "Blade/casing rubbing interactions in aircraft engines: numerical benchmark and design guidelines based on NASA rotor 37". In: Journal of Sound and Vibration Vol. 460 (2019), 114878. DOI: 10.1016/j.jsv.2019.114878. OAI: hal.archives-ouvertes.fr/hal-02281666.

[18] S. Kojtych, F. Nyssen, C. Audet, and A. Batailly. "Methodology for the Redesign of Compressor Blades Undergoing Nonlinear Structural Interactions: Application to Blade-Tip/Casing Contacts". In: Journal of Engineering for Gas Turbines and Power Vol. 145, No. 5 (2022). 051002. DOI: 10.1115/1.4055681. OAI: hal.archives-ouvertes.fr/hal-03795257.

[19] E. Piollet and A. Batailly. A program to compute compressor blade geometries from multiple-circular-arc parameters with sweep and lean(v1.0)[source code]. 2019. OAI: hal.archives-ouvertes.fr/hal-02127993.

[20] C. Monjaraz Tec, J. Gross, and M. Krack. "A massless boundary component mode synthesis method for elastodynamic contact problems". In: Computers and Structures Vol. 260 (2022), 106698. DOI: 10.1016/j.compstruc.2021.106698.

[21] Y. Hagita, H. Miyazawa, T. Furusawa, S. Yamamoto, K. Yonezawa, S. Umezawa, S. Ohmori, and T. Suzuki. "The Effect of Partial-Load Operation on a Gas Turbine Compressor of an Advanced Combined Cycle Power Plant". In: *Turbo Expo: Power for Land, Sea, and Air*. Vol. Volume 10D: Turbomachinery — Multidisciplinary Design Approaches, Optimization, and Uncertainty Quantification; Turbomachinery General Interest; Unsteady Flows in Turbomachinery. V10DT37A006. 2022, V10DT37A006. DOI: 10.1115/GT2022-80251.

[22] M. de Cherisey, L. Salles, L. Renson, A. Vizzaccaro, and C. Wong. "Optimization of a turbomachinery blade with regards to tip-rub events". In: *ASME Turbo Expo 2022: Turbine Technical Conference and Exposition*. 2022, V08BT27A013. DOI: 10.1115/GT2022-82005.

[23] J. Lainé, E. Piollet, F. Nyssen, and A. Batailly. "Blackbox optimization for aircraft engine bladed components featuring contact interfaces". In: Journal of Engineering for Gas Turbines and Power (2019). DOI: 10.1115/1.4042808. OAI: hal.archives-ouvertes.fr/hal-02059582/.

[24] S. Kojtych and A. Batailly. OpenMCAD, an open blade generator: from Multiple-Circular-Arc profiles to Computer-Aided Design model. Version 1.1. SWHID. oai:hal-03923093v2. Jan. 2023. OAI: hal.science/hal-03923093.

[25] J. E. Crouse, D. C. Janetzke, and R. E. Schwirian. *A computer program for composing compressor blading from simulated circular-arc elements on conical surfaces*. Tech. rep. NASA-TN-D-5437. NASA Lewis Research Center Cleveland, OH, United States, 1969. URL: https://ntrs.nasa.gov/citations/19690027504.

[26] L. Reid and R. D. Moore. *Design and overall performance of four highly loaded, high speed inlet stages for an advanced high-pressure-ratio core compressor*. Tech. rep. NASA-TP 1337. NASA Lewis Research Center Cleveland, OH, United States, 1978. URL: https://ntrs.nasa.gov/citations/19780025165.

[27] S. Kojtych and A. Batailly. A catalogue of open NASA blade models. Version 1.0. oai:hal-03945336. SWHID. Jan. 2023. OAI: hal.science/hal-03945336.

[28] D. C. Urasek, W. T. Gorrell, and W. S. Cunnan. *Performance of two-stage fan having low-aspect-ratio first-stage rotor blading*. Tech. rep. NASA-TP-1493. NASA Lewis Research Center Cleveland, OH, United States, 1979. URL: https://ntrs.nasa.gov/citations/19790018972.

[29] S. Kojtych. "Contributions à l'optimisation de systèmes mécaniques non réguliers : reconception d'aubes de compresseur". PhD thesis. Polytechnique Montréal, 2022. OAI: theses.hal.science/tel-03736103.

[30] Y. Colaïtis. "Stratégie numérique pour l'analyse qualitative des interactions aube/carter". PhD thesis. Montréal, QC, Canada: Dép. de génie mécanique, École Polytechnique de Montréal, 2021. OAI: tel.archives-ouvertes.fr/tel-03318777.

[31] C. J. Hulme, S. W. Fiebiger, and J. Szwedowicz. "Axial compressor blade failure, design modification, and its validation". In: *ASME Turbo Expo 2015: Turbine Technical Conference and Exposition*. Vol. 7A: Structures and Dynamics. Montréal, QC, Canada, 2015, V07AT28A011. DOI: 10.1115/GT2015-43312.

[32] R. R. Craig and M. C. C. Bampton. "Coupling of substructures for dynamic analyses". In: AIAA Journal Vol. 6, No. 7 (1968), 1313–1319. DOI: 10.2514/3.4741. OAI: hal.archives-ouvertes.fr/hal-01537654.

[33] S. Jain and G. Haller. "How to compute invariant manifolds and their reduced dynamics in high-dimensional finite element models". In: Nonlinear Dynamics Vol. 107, No. 2 (2022), 1417–1450. DOI: 10.1007/s11071-021-06957-4.

[34] G. Buza, S. Jain, and G. Haller. "Using spectral submanifolds for optimal mode selection in nonlinear model reduction". In: Proceedings of the Royal Society A: Mathematical, Physical and Engineering Sciences Vol. 477, No. 2246 (2021). Publisher: Royal Society, 20200725. DOI: 10.1098/rspa.2020.0725. URL: https://arxiv.org/abs/2009.04232.

[35] P. Benner, S. Gugercin, and K. Willcox. "A Survey of Projection-Based Model Reduction Methods for Parametric Dynamical Systems". In: SIAM Review Vol. 57, No. 4 (2015). Publisher: Society for Industrial and Applied Mathematics, 483–531. DOI: 10.1137/130932715. URL: https://kiwi.oden.utexas.edu/papers/Parametric-model-reduction-survey-Benner-Gugercin-Willcox.pdf.

[36] R. D. Hager and G. W. Lewis. *Effect of damper on overall and blade-element performance of a compressor rotor having a tip speed of 1151 feet per second and an aspect ratio of 3.6*. Tech. rep. NASA-TM X-3041. NASA Lewis Research Center Cleveland, OH, United States, 1974. URL: https://ntrs.nasa.gov/citations/19740018135.

[37] R. D. Hager, D. C. Janetzke, and L. Reid. *Performance of a 1380-foot-per-second-tip-speed axial-flow compressor rotor with a blade tip solidity of 1.3*. Tech. rep. NASA-TM X-2448. NASA Lewis Research Center Cleveland, OH, United States, 1972. URL: https://ntrs.nasa.gov/citations/19720012341.

[38] D. C. Janetzke, C. L. Ball, and R. D. Hager. *Performance of 1380-foot-per-second-tip-speed axial-flow compressor rotor with blade tip solidity of 1.1*. Tech. rep. NASA-TM X-2449. NASA Lewis Research Center Cleveland, OH, United States, 1972. URL: https://ntrs.nasa.gov/citations/19720011348.

[39] C. L. Ball, D. C. Janetzke, and L. Reid. *Performance of 1380-foot-per-second-tip-speed axial-flow compressor rotor with blade tip solidity of 1.5*. Tech. rep. NASA-TM X-2379. NASA Lewis Research Center Cleveland, OH, United States, 1972. URL: https://ntrs.nasa.gov/citations/19720007339.

[40] L. Reid and G. Kovich. *Overall and blade-element performance of a transonic compressor stage with multiple-circular-arc blades at tip speed of 419 meters per second*. Tech. rep. NASA-TM X-2731. NASA Lewis Research Center Cleveland, OH, United States, 1973. URL: https://ntrs.nasa.gov/citations/19730011268.

[41] D. C. Urasek and D. C. Janetzke. *Performance of tandem-bladed transonic compressor rotor with tip speed of 1375 feet per second*. Tech. rep. NASA-TM X-2484. NASA Lewis Research Center Cleveland, OH, United States, 1972. URL: https://ntrs.nasa.gov/citations/19720011123.

[42] W. M. Osborn, D. C. Urasek, and R. D. Moore. *Performance of a single-stage transonic compressor with a blade-tip solidity of 1.5 and comparison with 1.3- and 1.7-solidity stages*. Tech. rep. NASA-TM X-2926. NASA Lewis Research Center Cleveland, OH, United States, 1973. URL: https://ntrs.nasa.gov/citations/19740002621.

[43] G. Kovich, R. D. Moore, and D. C. Urasek. *Performance of transonic fan stage with weight flow per unit annulus area of 198 kilograms per sercond per square meter (40.6 (lb/sec)/ft²)*. Tech. rep. NASA-TM X-2905. NASA Lewis Research Center Cleveland, OH, United States, 1973. URL: https://ntrs.nasa.gov/citations/19740001915.

[44] L. Reid and R. D. Moore. *Performance of a single-stage transonic compressor with a blade-tip solidity of 1.7*. Tech. rep. NASA-TM X-2658. NASA Lewis Research Center Cleveland, OH, United States, 1972. URL: https://ntrs.nasa.gov/citations/19730006256.

[45] R. D. Moore, D. C. Urasek, and W. M. Osborn. *Performance of a single-stage transonic compressor with a blade-tip solidity of 1.3*. Tech. rep. NASA-TM X-2645. NASA Lewis Research Center Cleveland, OH, United States, 1972. URL: https://ntrs.nasa.gov/citations/19730002275.

[46] T. F. Gelder and G. W. Lewis. *Aerodynamic performance of 0.5-meter-diameter, 337-meter-per-second tip speed, 1.5-pressure-ratio, single-stage fan designed for low noise aircraft engines*. Tech. rep. NASA-TN D-7836. NASA Lewis Research Center Cleveland, OH, United States, 1974. URL: https://ntrs.nasa.gov/citations/19750006695.

[47] R. D. Moore, D. C. Urasek, and G. Kovlch. *Performance of transonic fan stage with weight flow per unit annulus area of 178 kilograms per sercond per square meter (36.5 (lb/sec)/ft²)*. Tech. rep. NASA-TM X-2904. NASA Lewis Research Center Cleveland, OH, United States, 1973. URL: https://ntrs.nasa.gov/citations/19740001906.

[48] D. C. Urasek, G. Kovich, and R. D. Moore. *Performance of transonic fan stage with weight flow per unit annulus area of 208 kilograms per sercond per square meter (42.6 (lb/sec)/ft²)*. Tech. rep. NASA-TM X-2903. NASA Lewis Research Center Cleveland, OH, United States, 1973. URL: https://ntrs.nasa.gov/citations/19740001910.

[49] G. W. Lewis, L. Reid, and E. R. Tysl. *Design and performance of a high-pressure-ratio, highly loaded axial-flow transonic compressor stage*. Tech. rep. NASA-TM X-3100. NASA Lewis Research Center Cleveland, OH, United States, 1974. URL: https://ntrs.nasa.gov/citations/19740025108.

[50] R. D. Moore, G. W. Lewis, and W. M. Osborn. *Performance of a Transonic Fan Stage Designed for a Low Meridional Velocity Ratio*. Tech. rep. NASA-TP-1298. NASA Lewis Research Center Cleveland, OH, United States, 1978. URL: https://ntrs.nasa.gov/api/citations/19780025164/downloads/19780025164.pdf.

[51] J. F. Schmidt and R. S. Ruggeri. *Performance With and Without Inlet Radial Distortion of a Transonic Fan Stage Designed for Reduced Loading in the Tip Region*. Tech. rep. NASA-TP-1294. NASA Lewis Research Center Cleveland, OH, United States, 1978. URL: https://ntrs.nasa.gov/citations/19780022114.

[52] W. R. Britsch, W. M. Osborn, and M. R. Laessig. *Effects of Diffusion Factor, Aspect Ratio, and Solidity on Overall Performance of 14 Compressor Middle Stages*. Tech. rep. NASA-TP-1523. NASA Lewis Research Center Cleveland, OH, United States, 1979. URL: https://ntrs.nasa.gov/citations/19790025039.

[53] L. Reid and R. D. Moore. *Performance of Single-Stage Axial-Flow Transonic Compressor With Rotor and Stator Aspect Ratios of 1.19 and 1.26, Respectively, and With Design Pressure Ratio of 1.82*. Tech. rep. NASA-TP-1338. NASA Lewis Research Center Cleveland, OH, United States, 1978. URL: https://ntrs.nasa.gov/citations/19790001889.

[54] L. Reid and R. D. Moore. *Performance of single-stage axial-flow transonic compressor with rotor and stator aspect ratios of 1.63 and 1.78, respectively, and with design pressure ratio of 1.82*. Tech. rep. NASA-TP-1974. NASA Lewis Research Center Cleveland, OH, United States, 1982. URL: https://ntrs.nasa.gov/citations/19820011348.

[55] R. D. Moore and L. Reid. *Performance of Single-Stage Axial-Flow Transonic Compressor With Rotor and Stator Aspect Ratios of 1.63 and 1.77, Respectively, and With Design Pressure Ratio of 2.05*. Tech. rep. NASA-TP-2001. NASA Lewis Research Center Cleveland, OH, United States, 1982. URL: https://ntrs.nasa.gov/citations/19820014395.

[56] W. M. Osborn and R. J. Steinke. *Performance of a 1.15-pressure-ratio Axial-flow Fan Stage with a Blade Tip Solidity of 0.5*. Tech. rep. NASA-TM X-3052. NASA Lewis Research Center Cleveland, OH, United States, 1974. URL: https://ntrs.nasa.gov/citations/19740021256.

[57] G. Kovich and R. J. Steinke. *Performance of a low-pressure-ratio low-tip-speed fan stage with blade tip solidity of 0.65*. Tech. rep. NASA-TM X-3341. NASA Lewis Research Center Cleveland, OH, United States, 1976. URL: https://ntrs.nasa.gov/citations/19760009985.

[58] R. D. Moore and R. J. Steinke. *Aerodynamic performance of a 1.25-pressure-ratio axial-flow fan stage*. Tech. rep. NASA-TM X-3083. NASA Lewis Research Center Cleveland, OH, United States, 1974. URL: https://ntrs.nasa.gov/citations/19740026337.

[59] W. M. Osborn, R. D. Moore, and R. J. Steinke. *Aerodynamic Performance of a 1.35-Pressure-Ratio Axial-Flow Fan Stage*. Tech. rep. NASA-TP-1299. NASA Lewis Research Center Cleveland, OH, United States, 1978. URL: https://ntrs.nasa.gov/citations/19790001851.

[60] G. W. Lewis and R. D. Moore. *Aerodynamic performance of a 1.20-pressure-ratio fan stage designed for low noise*. Tech. rep. NASA-TM X-3430. NASA Lewis Research Center Cleveland, OH, United States, 1976. URL: https://ntrs.nasa.gov/citations/19760026047.

[61] G. W. Lewis, R. D. Moore, and G. Kovich. *Performance of a 1.20-pressure-ratio STOL fan stage at three rotor blade setting angles*. Tech. rep. NASA-TM X-2837. NASA Lewis Research Center Cleveland, OH, United States, 1973. URL: https://ntrs.nasa.gov/citations/19730018974.

[62] R. D. Moore, G. Kovich, and E. R. Tysl. *Aerodynamic performance of 0.4066-scale model to JT8D refan stage*. Tech. rep. NASA-TM X-3356. NASA Lewis Research Center Cleveland, OH, United States, 1976. URL: https://ntrs.nasa.gov/citations/19760017065.

[63] D. C. Urasek, R. J. Steinke, and G. W. Lewis. *Performance of inlet stage of transonic compressor*. Tech. rep. NASA-TM X-3345. NASA Lewis Research Center Cleveland, OH, United States, 1976. URL: https://ntrs.nasa.gov/citations/19760009935.

[64] R. J. Steinke. *Design of 9.271-Pressure-Ratio Five-Stage Core Compressor and Overall Performance for First Three Stages*. Tech. rep. NASA-TP-2597. NASA Lewis Research Center Cleveland, OH, United States, 1986. URL: https://ntrs.nasa.gov/citations/19870008266.

[65] A. Batailly and A. Millecamps. "Minimising clearance consumption: a key factor for the design of blades robust to rotor/stator interactions ?" In: *ASME Turbo Expo 2016: Turbomachinery Technical Conference and Exposition*. Vol. 7A: Structures and Dynamics. Séoul, Corée du Sud, 2016, V07AT32A011. DOI: 10.1115/GT2016-56721. OAI: hal.archives-ouvertes.fr/hal-01618315.

[66] S. Le Digabel. "Algorithm 909: nomad: nonlinear optimization with the mads algorithm". In: Association for Computing Machinery Vol. 37, No. 4 (2011). DOI: 10.1145/1916461.1916468.

[67] C. Audet and J. E. Dennis Jr. "Mesh adaptive direct search algorithms for constrained optimization". In: SIAM Journal on Optimization Vol. 17, No. 1 (2006), 188–217. DOI: 10.1137/040603371. URL: https://scholarship.rice.edu/bitstream/handle/1911/102015/TR04-02.pdf.